Organometallic Halide Perovskites: Sharp Optical Absorption Edge and Its Relation to Photovoltaic Performance

Stefaan De Wolf,*,[†] Jakub Holovsky,[‡] Soo-Jin Moon,[§] Philipp Löper,[†] Bjoern Niesen,[†] Martin Ledinsky,[†,‡] Franz-Josef Haug,[†] Jun-Ho Yum,[§] and Christophe Ballif[†,§]

[†]Photovoltaics and Thin-Film Electronics Laboratory, Institute of Microengineering (IMT), Ecole Polytechnique Fédérale de Lausanne (EPFL), Maladière 71, Neuchâtel 2000, Switzerland
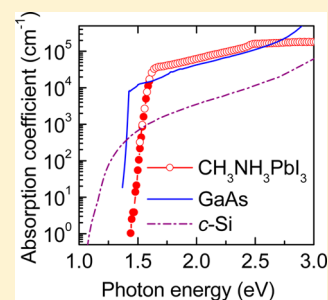
[‡]Institute of Physics, Academy of Sciences of the Czech Republic, v. v. i., Cukrovarnická 10, 162 00 Prague, Czech Republic

[§]PV Center, Centre Suisse d'Electronique et de Microtechnique (CSEM), Jacquet Droz 1, Neuchâtel 2000, Switzerland

S *Supporting Information*

ABSTRACT: Solar cells based on organometallic halide perovskite absorber layers are emerging as a high-performance photovoltaic technology. Using highly sensitive photothermal deflection and photocurrent spectroscopy, we measure the absorption spectrum of $CH_3NH_3PbI_3$ perovskite thin films at room temperature. We find a high absorption coefficient with particularly sharp onset. Below the bandgap, the absorption is exponential over more than four decades with an Urbach energy as small as 15 meV, which suggests a well-ordered microstructure. No deep states are found down to the detection limit of ~1 cm^{-1}. These results confirm the excellent electronic properties of perovskite thin films, enabling the very high open-circuit voltages reported for perovskite solar cells. Following intentional moisture ingress, we find that the absorption at photon energies below 2.4 eV is strongly reduced, pointing to a compositional change of the material.

SECTION: Energy Conversion and Storage; Energy and Charge Transport

Large-scale deployment of terrestrial photovoltaics critically depends on devices with high energy-conversion efficiencies at acceptable cost. Very recently, organometallic halide perovskite ($CH_3NH_3PbX_3$, X = halogen)-based solar cells have attracted significant attention as promising candidates to fulfill these requirements.[1−4] Kojima et al. pioneered the field by replacing the dye in iodide/triiodide liquid electrolyte-based TiO_2 mesoscopic solar cells with $CH_3NH_3PbBr_3$ and $CH_3NH_3PbI_3$ perovskites and demonstrated power conversion efficiencies (PCEs) of 3.1 and 3.8%, respectively.[5] In 2012, a strong efficiency improvement to 9% was achieved by replacing the liquid electrolyte with a solid-state hole-transport material, 2,2′,7,7′-tetrakis(*N,N*-di-*p*-methoxyphenylamine)-9,9′-spirobifluorene (spiro-MeOTAD).[6] This development initiated rapid progress in device performance, with current efficiencies well above 15%, reported by various groups.[7−9] Moreover, whereas initial research focused on the implementation of organometallic halide perovskite layers in mesoscopic solar cells by replacing the organic dye as the light absorber material,[5,10] recently it was shown that highly efficient perovskite-based solar cells without a mesoscopic scaffold can be realized.[8,9,11−14]

Particularly striking are the remarkably high open-circuit voltages, V_{OC} (up to 1.13 V to date),[11] that are obtained for iodide-based perovskite solar cells compared with their optical bandgap, E_G (~1.57 eV).[15] This is largely irrespective of their deposition method, which can be either solution- or vacuum-processed. Quite generally, the bandgap-voltage offset $(E_G/q) − V_{OC}$, where q is the elementary charge, is a useful measure to

assess the electronic quality of the absorber in a solar cell,[16,17] including perovskites.[18] This offset directly scales with detrimental recombination losses in the device, such as those via deep defects or interfaces. Further insight into the potential of a material as a photovoltaic absorber can be gained from its optical band edges and sub-bandgap absorption spectrum. Photothermal deflection spectroscopy (PDS) and Fourier-transform photocurrent spectroscopy (FTPS) are appropriate methods to determine these optical properties; they allow for the measurement of absorbances over several orders of magnitude with sensitivities down to 10^{-4} for PDS and 10^{-6} for FTPS and have extensively been used to analyze electronic defects in amorphous silicon[19−21] as well as organic semiconductors.[22]

Here we present the optical absorption edge and sub-bandgap absorption of thin films of solution-processed organometallic halide perovskite $CH_3NH_3PbI_3$, demonstrating that PDS and FTPS spectroscopy can reliably be applied to perovskite layers. We find remarkably sharp absorption edges with no apparent presence of deep states. Moreover, we report on the effect of moisture ingress on the absorption spectrum. Finally, we point out consequences of our findings for future device development.

The absorptance spectrum of an as-prepared $CH_3NH_3PbI_3$ perovskite thin film on glass measured by PDS, is shown in Figure 1. It exhibits a remarkably steep absorptance onset at a

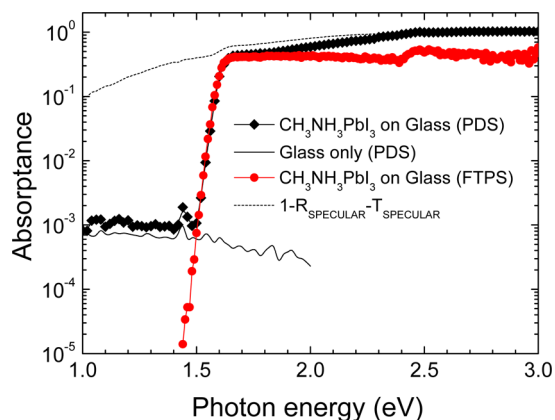**Figure 1.** PDS, FTPS, and $1 - R_{specular} - T_{specular}$ spectra of $CH_3NH_3PbI_3$ perovskite thin films as well as the PDS spectra of the glass substrate, all measured at room temperature. Film thickness d_{eff} = 220 nm.

photon energy of ~1.5 eV, with a rising absorptance until a sharp shoulder appears at a photon energy near its reported bandgap, following which it saturates for photon energies above ~2.45 eV. Near this absorptance onset, at 1.40 to 1.55 eV, the absorptance spectrum features an exponential increase. Figure 1 also shows the spectrum of the bare glass substrate, which clearly indicates that the sub-bandgap absorption sensitivity of our PDS measurements of the as-prepared $CH_3NH_3PbI_3$ layer is fully limited by defects present in the glass substrate.

To gain more information about the sub-bandgap absorption of the $CH_3NH_3PbI_3$ layer at photon energies below 1.5 eV, we performed FTPS measurements. In contrast with PDS, the FTPS signal is free of any substrate contribution. This is because absorption in the glass substrate at energies below the glass bandgap does not induce free charge carriers and therefore does not contribute to the photocurrent collected during FTPS measurements. Several important points ensue from the FTPS spectrum of the $CH_3NH_3PbI_3$ layer, shown in Figure 1. First, because of the nature of the characterization technique involved, this measurement proves that the perovskite material has a sufficiently high photosensitivity to generate a photocurrent that is significant compared with its dark current. Second, the FTPS spectrum features the same steep onset and sharp bending of the $CH_3NH_3PbI_3$ absorptance as the PDS spectrum. Third, the FTPS curve does not saturate for photon energies below 1.5 eV, but continues to decrease to values as low as 10^{-5}. Finally, for planar FTPS, recombination of photoexited carriers close to the surface can diminish the response in the visible-UV part of the spectrum. This is an effect that does not seem to be pronounced here, thus implying low surface recombination.

We obtain further insight into the relevance of the absorption spectrum by plotting the absorption coefficient of the $CH_3NH_3PbI_3$ perovskite film, as shown in Figure 2. Because we cannot fully exclude light scattering at the surface roughness, we plot only the effective absorption coefficient, α_{eff}, corresponding to a layer thickness d_{eff} = 220 nm, considering the surrounding medium and surface roughness. This coefficient was calculated from the measured data given in

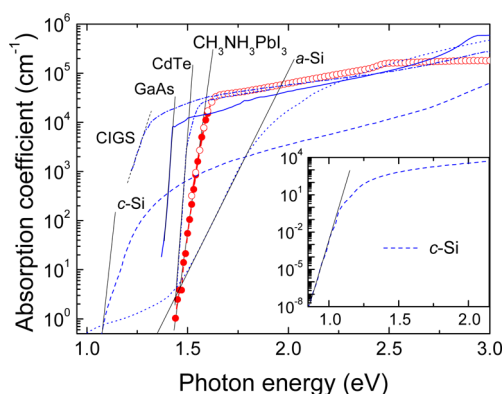**Figure 2.** Effective absorption coefficient of a $CH_3NH_3PbI_3$ perovskite thin film compared with other typical photovoltaic materials, including amorphous silicon (*a*-Si), GaAs, CIGS, CdTe, and crystalline silicon (*c*-Si), all measured at room temperature. For each material, we show the slope of the Urbach tail. For clarity, the inset shows the data for *c*-Si down to low absorption values.

Figure 1, using the formula $\alpha_{eff} = d_{eff}^{-1} \ln(1 + A_{PDS}/T_{specular})$, for the case of a negligible film-glass reflectance.[23] (See the Supporting Information for further details.) We also show in this Figure the absorption coefficients of several other market-relevant photovoltaic materials taken from literature, including GaAs,[24] CdTe,[24] CIGS,[25] crystalline silicon (*c*-Si),[26] and amorphous silicon (*a*-Si, own data). Previously, it was already inferred from the so-called Tauc plot of the absorption curve that iodide perovskites have a direct bandgap,[27] in agreement with recent calculations.[28] Analyzing now the data in Figure 2, we find three new striking results.

First, the curve of the perovskite absorption coefficient shows an unusual sharp shoulder near its reported bandgap value (~1.57 eV). It is particularly remarkable that this shoulder occurs at higher absorption coefficients than most other comparable semiconductors. This explains why very thin absorber films suffice for perovskite solar cell fabrication.

Second, below this shoulder, the absorption coefficient of the perovskite follows a purely exponential trend without much deviation toward lower photon energies. The slope of this exponential part of the curve is the so-called Urbach energy,[29] E_0, and equals 15 meV, which is a low value. This slope represents the absorption tail states (also called Urbach tail) of the $CH_3NH_3PbI_3$ perovskite film. Compared with the other semiconductors shown in Figure 2, we see that the Urbach energy of the $CH_3NH_3PbI_3$ perovskite is close to the values of GaAs, a monocrystalline direct-bandgap semiconductor of very high electrical quality. The absorption spectrum of *c*-Si shows a similar slope as well below its bandgap, but because the bandgap is indirect, it occurs at much lower values and shows signatures related to phonon-assisted absorption. (See the inset in Figure 2.) In general, when the temperature decreases, the slope of the Urbach tail of a crystalline material diminishes with the reduced degree of thermal disorder, which scales with kT (with Boltzmann's constant, k, and the absolute temperature, T). The temperature dependence of the Urbach tail is also well known for *a*-Si, with a temperature-independent offset of ~40 to 45 meV, explaining the large values associated with this material, seen also in Figure 2. This broadening of the Urbach energy is generally attributed to inherent structural disorder of the material.[30] The low value measured for the $CH_3NH_3PbI_3$

perovskite film suggests a very low degree of structural disorder and therefore crystalline nature of the film.

Third, the fact that the Urbach tail shows a purely exponential trend over more than four decades, even for the lowest measured values, strongly suggests that no optically detectable deep states are present in the $CH_3NH_3PbI_3$ material (clearly contrasting with a-Si). This observation is likely a key factor in the understanding why perovskite solar cells can feature such high V_{OC} values compared with their bandgap.

An equally important factor explaining the high V_{OC} values for perovskite solar cells can likely be found in the small value measured for its Urbach energy. In Figure 3, we plot $(E_G/q) -$

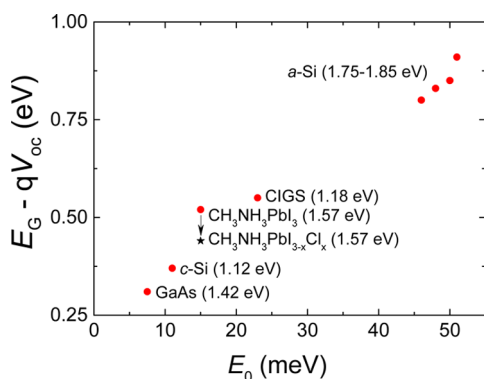**Figure 3.** $(E_G/q) - V_{OC}$ versus Urbach energy for typical photovoltaic absorber materials at room temperature. For each material, we also indicate the value of E_G.

V_{OC} as function of E_0 for a range of photovoltaic materials taken from literature. We took for these materials the highest reported V_{oc} values (c-Si, 0.75 V;[31] GaAs, 1.12 V;[32] $CH_3NH_3PbI_3$ perovskites, 1.05 V),[9] whereas for the Urbach energy we took the smallest reported values at room temperature (c-Si, 11 meV, fitted from literature data;[26] GaAs, 7.5 meV;[33] and $CH_3NH_3PbI_3$ perovskites, 15 meV, this work). Owing to the greater variability in a-Si, CIGS, and CdTe, we quote only data where all parameters have been measured consistently on the same set of samples.[34,35] It is important to bear in mind that besides the nature (amorphous vs crystalline) and purity of a material, the V_{oc} also depends on the type of bandgap (direct vs indirect), the absorber thickness, and the specific solar-cell architecture. As an example, the carrier-selective contacts have been argued to play a key role in explaining the high V_{OC} in perovskite solar cell.[36,37] Besides this, an empirical trend emerges from Figure 3, where materials with the smallest Urbach energy lead to the lowest $(E_G/q) - V_{OC}$ values. The $CH_3NH_3PbI_3$ perovskite cells are approaching the best c-Si and GaAs solar cells, the latter devices making use of sophisticated processes combined with perfectly grown crystalline absorbers. To show the full potential of iodide-based perovskite devices, we also include data of mixed-halide $CH_3NH_3PbI_{3-x}Cl_x$ perovskites in this Figure, assuming they have the same Urbach energy as measured here for the $CH_3NH_3PbI_3$ perovskites. Mixed-halide devices have the highest reported V_{OC} to date (1.13 V),[11] while their bandgap is the same as that for $CH_3NH_3PbI_3$ perovskites.[27] We also remark that for wider-bandgap $CH_3NH_3PbBr_3$ perovskite-based solar cells (E_G = 2.3 eV) even higher V_{OC} values were reported (1.5 eV, with chloride inclusion in the absorber).[38] The bandgap–voltage offset $(E_G/q) - V_{OC}$ is higher for this

material, which likely can be lowered by tailoring the device interface energetics, however.[39]

For the application of organometallic halide perovskites in solar cells, their stability against light-, humidity-, or oxygen-induced degradation is an indispensable prerequisite. The perovskite materials that have been developed so far are known to degrade upon exposure to, for example, humidity.[40] The number of detailed degradation studies is limited, however. For example, it is not well known to which extent the material changes when measured at ambient atmosphere or when exposed to liquids.

Here we verified the effect of Fluorinert FC-72 (C_6F_{14}), in which the sample is immersed during PDS measurements, on the $CH_3NH_3PbI_3$ layer and found that even after exposure to the liquid for 24 h the PDS spectrum did not significantly change. This implies not only that the $CH_3NH_3PbI_3$ layer is chemically stable in the FC-72 liquid but also that this liquid efficiently protects the perovskite layer from the ambient atmosphere and prevents degradation of its optical properties. Because the perovskite layer exhibits excellent stability when immersed in FC-72, PDS proves to be a highly suitable method to investigate organometallic halide perovskites as-deposited as well as in degraded states.

In Figure 4, we show PDS spectra of $CH_3NH_3PbI_3$ layers after exposure to ambient air with 30−40% relative humidity

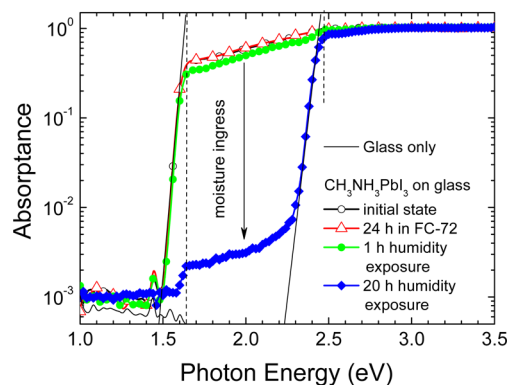**Figure 4.** PDS spectra of $CH_3NH_3PbI_3$ perovskite thin films during prolonged immersion in the FC-72 solution and following moisture exposure.

during 1 and 20 h, respectively. Following moisture exposure, the material is bleached and has a pale yellow-whitish appearance. The Figure shows that the absorptance between photon energies of 1.5 and 2.5 eV drops by two orders of magnitude. The spectral position of the absorption onset at 2.3 eV corresponds to the bandgap of PbI_2,[14] which may indicate that $CH_3NH_3PbI_3$ can decompose into PbI_2 in a humid ambient due to the dissolution of disordered CH_3NH_3I.[40,4] To precisely understand the impact of moisture exposure on the crystalline structure and chemical composition of $CH_3NH_3PbI_3$ layers, further research by methods such as X-ray diffraction spectroscopy, X-ray photoelectron spectroscopy or transmission electron microscopy is required. It is noteworthy that recently cells with a mixed halide (Br with I) were reported to show improved stability, and material measured after exposure to ambient air with 55% relative humidity for 1 day did not show changes in X-ray diffraction patterns.[40]

Regarding the stability under light exposure, native deep-defect formation under visible-light soaking is of serious

concern in *a*-Si solar cells. This phenomenon — commonly referred to as the Staebler−Wronski effect[41] — can be convincingly explained by the disorder-induced broadening of the Urbach tail in this material, where strained Si−Si bonds can rupture into two Si dangling bonds, acting as recombination sites.[42] The low Urbach energy measured here for $CH_3NH_3PbI_3$ perovskites, likely not featuring any disorder-induced broadening, may be a strong indicator that this material will not suffer from a similar phenomenon. Promising long-term results were indeed reported for such a solar cell when well-encapsulated, maintaining 80% of its initial conversion efficiency, following 500 h of maximum power operation at approximately sunlight intensity.[7]

Finally, the high voltage and ease of processing of perovskite solar cells were already pointed out as two factors that may motivate the integration of perovskite solar cells into tandem configurations, featuring either *c*-Si or CIGS bottom cells.[18] The absence of detectable sub-bandgap absorption below photon energies of 1.5 eV for perovskites (meaning the material is highly transparent for optical wavelengths above ∼825 nm) may further advocate the development of such devices.

In summary, motivated by the excellent low-bandgap−open-circuit voltage offsets reported for organometallic halide perovskite solar cells, we presented the band-edge and sub-bandgap absorption spectrum of $CH_3NH_3PbI_3$ perovskite thin films. We showed that both PDS as well as FTPS are ideally suited techniques for this purpose. We find that the $CH_3NH_3PbI_3$ perovskite has a particularly steep absorption onset, with an Urbach energy of 15 meV. The optical absorption edges are purely exponential, over more than four decades of absorption coefficient values, with the absence of optically detected deep states. Upon moisture ingress, the strong absorption onset of the material shifts from ∼1.6 to almost 2.4 eV, where the shape of the absorptance spectrum suggests a compositional change of the deposited material. Finally, the $CH_3NH_3PbI_3$ perovskite was found to be highly transparent for optical wavelengths larger than 825 nm, further underlining the appeal of integrating such solar cells into stacked tandem devices.

■ ASSOCIATED CONTENT

ⓈSupporting Information

Experimental methods including sample preparation and characterization. Discussion on the differences between the FTPS and PDS methods and the effect of light scattering.

This material is available free of charge via the Internet at http://pubs.acs.org.

■ AUTHOR INFORMATION

Corresponding Author
*E-mail: stefaan.dewolf@epfl.ch.

Notes
The authors declare no competing financial interests.

■ ACKNOWLEDGMENTS

■ REFERENCES

(1) Hodes, G. Perovskite-Based Solar Cells. *Science* **2013**, *342*, 317−318.

(2) Park, N.-G. Organometal Perovskite Light Absorbers Toward a 20% Efficiency Low-Cost Solid-State Mesoscopic Solar Cell. *J. Phys. Chem. Lett.* **2013**, *4*, 2423−2429.

(3) Kamat, P. V. Evolution of Perovskite Photovoltaics and Decrease in Energy Payback Time. *J. Phys. Chem. Lett.* **2013**, *4*, 3733−3734.

(4) Kim, H. S.; Im, S. H.; Park, N. G. Organolead Halide Perovskite: New Horizons in Solar Cell Research. *J. Phys. Chem. C* **2014**, DOI: 10.1021/jp409025w.

(5) Kojima, A.; Teshima, K.; Shirai, Y.; Miyasaka, T. Organometal Halide Perovskites as Visible-Light Sensitizers for Photovoltaic Cells. *J. Am. Chem. Soc.* **2009**, *131*, 6050−6051.

(6) Kim, H.-S.; Lee, C.-R.; Im, J.-H.; Lee, K.-B.; Moehl, T.; Marchioro, A.; Moon, S.-J.; Humphry-Baker, R.; Yum, J.-H.; Moser, J. E.; et al. Lead Iodide Perovskite Sensitized All-Solid-State Submicron Thin Film Mesoscopic Solar Cell with Efficiency Exceeding 9%. *Sci. Rep.* **2012**, *2* (591), 1−7.

(7) Burschka, J.; Pellet, N.; Moon, S.-J.; Humphry-Baker, R.; Gao, R. P.; Nazeeruddin, M. K.; Graetzel, M. Sequential Deposition as a Route to High-Performance Perovskite-Sensitized Solar Cells. *Nature* **2013**, *499*, 316−319.

(8) Liu, M. Z.; Johnston, M. B.; Snaith, H. J. Efficient Planar Heterojunction Perovskite Solar Cells by Vapour Deposition. *Nature* **2013**, *501*, 395−398.

(9) Malinkiewicz, O.; Yella, A.; Lee, Y. H.; Minguez Espallargas, G.; Graetzel, M.; Nazeeruddin, M. K.; Bolink, H. J. Perovskite Solar Cells Employing Organic Charge-Transport Layers. *Nat. Photon.* **2014**, *8*, 128−132.

(10) Im, J.-H.; Lee, C.-R.; Lee, J.-W.; Park, S.-W.; Park, N.-G. 6.5% Efficient Perovskite Quantum-Dot-Sensitized Solar Cell. *Nanoscale* **2011**, *3*, 4088−4093.

(11) Lee, M. M.; Teuscher, J.; Miyasaka, T.; Murakami, T. N.; Snaith, H. J. Efficient Hybrid Solar Cells Based on Meso-Superstructured Organometal Halide Perovskites. *Science* **2012**, *338*, 643−647.

(12) Jeng, J.-Y.; Chiang, Y.-F.; Lee, M.-H.; Peng, S.-R.; Guo, T.-F.; Chen, P.; Wen, T.-C. $CH_3NH_3PbI_3$ Perovskite/Fullerene Planar-Heterojunction Hybrid Solar Cells. *Adv. Mater.* **2013**, *25*, 3727−3732.

(13) Abrusci, A.; Stranks, S. D.; Docampo, P.; Yip, H.-L.; Jen, A.K.-Y.; Snaith, H. J. High-Performance Perovskite-Polymer Hybrid Solar Cells via Electronic Coupling with Fullerene Monolayers. *Nano Lett.* **2013**, *13*, 3124−3128.

(14) Liu, D.; Kelly, T. L. Perovskite Solar Cells with a Planar Heterojunction Structure Prepared using Room-Temperature Solution Processing Techniques. *Nat. Photon* **2014**, *8*, 133−138.

(15) Eperon, G. E.; Stranks, S. D.; Menelaou, C.; Johnston, M. B.; Herz, L. M.; Snaith, H. J. Formamidinium Lead Trihalide: a Broadly Tunable Perovskite for Efficient Planar Heterojunction Solar Cells. *Energy Environ. Sci.* **2014**, *7*, 982−988.

(16) Tiedje, T.; Yablanovitch, E.; Cody, G. D.; Brooks, B. G. Limiting Efficiency of Silicon Solar Cells. *IEEE Trans. Electron Devices* **1984**, *31*, 711−716.

(17) King, R. R.; Bhusari, D.; Boca, A.; Larrabee, D.; Liu, X. Q.; Hong, W.; Fetzer, C. M.; Law, D. C.; Karam, N. H. Band Gap - Voltage Offset and Energy Production in Next-Generation Multi-junction Solar Cells. *Prog. Photovoltaics* **2011**, *19*, 797−812.

(18) Snaith, H. J. Perovskites: The Emergence of a New Era for Low-Cost, High-Efficiency Solar Cells. *J. Phys. Chem. Lett.* **2013**, *4*, 3623−3630.

(19) Jackson, W. B.; Amer, N. M. Direct Measurement of Gap-State Absorption in Hydrogenated Amorphous Silicon by Photothermal Deflection Spectroscopy. *Phys. Rev. B* **1982**, *25*, 5559−5562.

(20) Vaněček, M.; Poruba, A. Fourier-Transform Photocurrent Spectroscopy of Microcrystalline Silicon for Solar Cells. *Appl. Phys. Lett.* **2002**, *80*, 719−721.

(21) Holovský, J.; Schmid, M.; Stuckelberger, M.; Despeisse, M.; Ballif, C.; Poruba, A.; Vaněček, M. Time Evolution of Surface Defect States in Hydrogenated Amorphous Silicon studied by Photothermal

and Photocurrent Spectroscopy and Optical Simulation. *J. Non-Cryst. Solids* **2012**, *358*, 2035−2038.

(22) Vandewal, K.; Gadisa, A.; Oosterbaan, W. D.; Bertho, S.; Banishoeib, F.; Van Severen, I.; Lutsen, L.; Cleij, T. J.; Vanderzande, D.; Manca, J. V. The Relation Between Open-Circuit Voltage and the Onset of Photocurrent Generation by Charge-Transfer Absorption in Polymer: Fullerene Bulk Heterojunction Solar Cells. *Adv. Funct. Mater.* **2008**, *18*, 2064−2070.

(23) Ritter, D.; Weiser, K. Suppression of Interference Fringes in Absorption Measurements on Thin Films. *Opt. Commun.* **1986**, *57*, 336−338.

(24) Palik, E. D. *Handbook of Optical Constants of Solids*; Academic Press: San Diego, CA, 1998.

(25) Minoura, S.; Kodera, K.; Maekawa, T.; Miyazaki, K.; Niki, S.; Fujiwara, H. Dielectric Function of $Cu(In, Ga)Se_2$-Based Polycrystalline Materials. *J. Appl. Phys.* **2013**, *113* (063505), 1−14.

(26) Green, M. A. Self-Consistent Optical Parameters of Intrinsic Silicon at 300 K including Temperature Coefficients. *Sol. Energy Mater. Sol. Cells* **2008**, *92*, 1305−1310.

(27) Colella, S.; Mosconi, E.; Fedelli, P.; Listorti, A.; Gazza, F.; Orlandi, F.; Ferro, P.; Besagni, T.; Rizzo, A.; Calestani, F.; et al. $MAPbI_{3-x}Cl_x$ Mixed Halide Perovskite for Hybrid Solar Cells: The Role of Chloride as Dopant on the Transport and Structural Properties. *Chem. Mater.* **2013**, *25*, 4613−4618.

(28) Brivio, F.; Walker, A. B.; Walsch, A. Structural and Electronic Properties of Hybrid Perovskites for High-Efficiency Thin-Film Photovoltaics from First-Principles. *APL Mater.* **2013**, *1* (042111), 1−5.

(29) Urbach, F. The Long-Wavelength Edge of Photographic Sensitivity and of the Electronic Absorption of Solids. *Phys. Rev.* **1953**, *92*, 1324−1324.

(30) Cody, G. D.; Tiedje, T.; Abeles, B.; Brooks, B.; Goldstein, Y. Disorder and the Optical-Absorption Edge of Hydrogenated Amorphous Silicon. *Phys. Rev. Lett.* **1981**, *47*, 1480−1483.

(31) Taguchi, M.; Yano, A.; Tohoda, S.; Matsuyama, K.; Nakamura, Y.; Nishiwaki, T.; Fujita, K.; Maruyama, E. 24.7% Record Efficiency HIT Solar Cell on Thin Silicon Wafer. *IEEE J. Photovoltaics* **2014**, *4*, 96−99.

(32) Miller, O. D.; Yablonovitch, E.; Kurtz, S. R. Strong Internal and External Luminescence as Solar Cells Approach the Shockley−Queisser Limit. *IEEE J. Photovoltaics* **2012**, *2*, 303−311.

(33) Johnson, S. R.; Tiedje, T. Temperature Dependence of the Urbach Edge in GaAs. *J. Appl. Phys.* **1995**, *78*, 5609−5613.

(34) van Veen, M. K.; Schropp, R. E. I. Beneficial Effect of a Low Deposition Temperature of Hot-Wire Deposited Intrinsic Amorphous Silicon for Solar Cells. *J. Appl. Phys.* **2003**, *93*, 121−125.

(35) Heath, J. T.; Cohen, J. D.; Shafarman, W. N.; Liao, D. X.; Rockett, A. A. Effect of Ga Content on Defect States in $CuIn_{1-x}Ga_xSe_2$ Photovoltaic Devices. *Appl. Phys. Lett.* **2002**, *80*, 4540−4542.

(36) Bi, D.; Yang, L.; Boschloo, G.; Hagfeldt, A.; Johansson, E. M. J. Effect of Different Hole Transport Materials on recombination in $CH_3NH_3PbI_3$ Perovskite-Sensitized Mesoscopic Solar Cells. *J. Phys. Chem. Lett.* **2013**, *4*, 1532−1536.

(37) Juarez-Perez, E. J.; Wußler, M.; Fabregat-Santiago, F.; Lakus-Wollny, K.; Mankel, E.; Mayer, T.; Jaegermann, W.; Mora-Sero, I. Role of the Selective Contacts in the Performance of Lead Halide Perovskite Solar Cells. *J. Phys. Chem. Lett.* **2014**, *5*, 680−685.

(38) Edri, W.; Kirmayer, S.; Kulbak, M.; Hodes, G.; Cahen, D. Chloride Inclusion and Hole Transport Material Doping to Improve Methyl Ammonium Lead Bromide Perovskite-Based High Open-Circuit Voltage Solar Cells. *J. Phys. Chem. Lett* **2014**, *5*, 429−433.

(39) Schulz, P.; Edri, E.; Kirmayer, S.; Hodes, G.; Cahen, D.; Kahn, A. Interface Energetics in Organo-Metal Halide Perovskite-Based Photovoltaic Cells. *Energy Environ. Sci.* **2014**, DOI: 10.1039/c4ee00168k.

(40) Noh, J. H.; Im, S. H.; Heo, J. H.; T.N. Mandal, T. N.; Seok, S. I. Chemical Management for Colorful, Efficient, and Stable Inorganic−Organic Hybrid Nanostructured Solar Cells. *Nano Lett.* **2013**, *13*, 1764−1769.

(41) Staebler, D. L.; Wronski, C. R. Reversible Conductivity Changes in Discharge-Produced Amorphous Si. *Appl. Phys. Lett.* **1977**, *31*, 292−294.

(42) Stutzmann, M.; Jackson, W. B.; Tsai, C. C. Light-Induced Metastable Defects in Hydrogenated Amorphous Silicon: A Systematic Study. *Phys. Rev. B.* **1985**, *32*, 23−47.